# Description of fusion and evaporation residue formation cross sections in reactions leading to the formation of element $Z = 122$ within the Langevin approach

V. L. Litnevsky* and G. I. Kosenko†
*Omsk Tank Automotive Engineering Institute, Omsk, Russia*

F. A. Ivanyuk‡
*Institute for Nuclear Research, Kiev, Ukraine*

(Received 7 December 2015; published 13 June 2016)

We describe the evolution of the compact system formed by the touching of two colliding ions in reactions $^{58}\mathrm{Fe}+{}^{248}\mathrm{Cm}\rightarrow{}^{306-x}122+xn$, $^{64}\mathrm{Ni}+{}^{244}\mathrm{Pu}\rightarrow{}^{308-x}122+xn$, and $^{90}\mathrm{Zr}+{}^{208}\mathrm{Pb}\rightarrow{}^{298-x}122+xn$. The description is carried out within the dynamical multidimensional stochastic approach, based on Langevin equations for the shape degrees of freedom of colliding ions and the compact system. For the approach stage we take into account the shell structure of colliding ions, their orientation in the space, and the effect of tunneling of ions through the Coulomb barrier. By describing the evolution of the compact system formed after the touching of incident ions, the shell structure of the compact system is also taken into account. Within this approach we have calculated the compound nucleus and evaporation residue formation cross sections. These can be compared with the experimental data. We have also clarified the impact of the tunneling effect in the entrance channel on the fusion and evaporation residue cross sections.

DOI: 10.1103/PhysRevC.93.064606

## I. INTRODUCTION

The synthesis of superheavy elements and the investigation of their properties is one of the most important problems of modern nuclear physics. Since the probability of superheavy element formation is extremely small, the theoretical estimation of the corresponding cross sections and prediction of the optimal choice of the target and projectile nuclei are of great interest.

In our previous publications, see Ref. [1] and references therein, we have developed a two-step approach for the description of fusion-fission reactions. In the first step (the entrance channel) the time evolution of the system up to the touching point is described. The distributions at the touching point obtained in the first step are used for the transition from separated ions to the compact system and as the initial conditions for the description of the evolution of the compact system (second step).

Both the approach of ions and the evolution of the compact system (up to the formation of evaporation residue) are described with help of Langevin equations for the collective coordinates (deformation parameters) which specify the shape of the nuclear system. In both stages the shell structure of colliding ions and compound nucleus is taken into account.

In recent publication [2] we considered the approach phase of ions leading to the formation of superheavy elements with charge numbers between $Z = 112$ and $Z = 122$. The comparison of calculated results with the available experimental data [3] has shown that by describing the process of ion collision one should take into account not only the deformation [1,4] and reciprocal orientation of ions [5,6], but also the possibility of tunneling through the Coulomb barrier [1,7].

The capture (touching) cross section calculated in [2] for the reactions $^{58}\mathrm{Fe}+{}^{248}\mathrm{Cm}\rightarrow{}^{306-x}122+xn$ leading to synthesis of isotopes with $Z = 122$ was found to be rather close to the experimental data [3] available at the reaction energy 33 MeV ($E_{\mathrm{cm}} = 279$ MeV).

In [2] the touching cross sections in other reactions, $^{64}\mathrm{Ni}+{}^{244}\mathrm{Pu}\rightarrow{}^{308-x}122+xn$, $^{90}\mathrm{Zr}+{}^{208}\mathrm{Pb}\rightarrow{}^{298-x}122+xn$, leading to the synthesis of isotopes with $Z = 122$ were also analyzed. It was shown that the touching cross sections in these reactions are larger for mass symmetric combinations of the projectile and target nuclei. On the other hand, it follows from the earlier works [8,9] that the fusion (the penetration through the fission barrier toward the ground state) probability for the mass symmetric combination of the projectile and target is strongly suppressed. Thus the description of the whole process from the approaching stage till the formation of the evaporation residue is necessary in order to predict the most favorable combination of the target and projectile nuclei.

In present work we analyze the evolution of the compact systems formed in reactions $^{58}\mathrm{Fe}+{}^{248}\mathrm{Cm}\rightarrow{}^{306-x}122+xn$, $^{64}\mathrm{Ni}+{}^{244}\mathrm{Pu}\rightarrow{}^{308-x}122+xn$, and $^{90}\mathrm{Zr}+{}^{208}\mathrm{Pb}\rightarrow{}^{298-x}122+xn$ from the touching point up to the formation of the evaporation residue. The distributions at the touching point obtained in [2] are used as the initial conditions for the time evolution of compact system.

By solving Langevin equations for the shape degrees of freedom, we have calculated the fusion and evaporation residue formation cross sections for these reactions at various reaction energies, and we have clarified the role of mass asymmetry of colliding nuclei on the formation of compound nucleus and the role of the tunneling effect in the entrance channel.

*vlad.lit@bk.ru
†kosenkophys@gmail.com
‡ivanyuk@kinr.kiev.ua

 

The penetrability of the barrier was defined in the WKB approximation, i.e.,

$$T_L(E) = \left[1 + \exp\left(\frac{2}{\hbar}\int_{r_2}^{r_1}\sqrt{2m(V^{\rm fus} - E)}dr\right)\right]^{-1}, \quad (1)$$

where the integration is carried out between the turning points $r_1$ and $r_2$ in the subbarrier region and $E$ is the potential energy of the system at the turning points. One can find more details in [7].

## II. THE REACTION MODEL

We describe the shape of the compact system formed after the touching of projectile and target nuclei by means of the Cassini shape parametrization [10,11] and take into account three deformation parameters, namely, $\alpha$, $\alpha_1$, and $\alpha_4$. These parameters fix the elongation of the system, the mass asymmetry, and the neck radius, repectively. For the spherical shape $\alpha = \alpha_1 = \alpha_4 = 0$. The touching point configuration of the system can be parametrized by $\alpha = 1$ (zero neck radius condition); the $\alpha_1$ and $\alpha_4$ parameters at the touching point are fixed by the mass asymmetry of the colliding nuclei and the requirement that the value of potential energy of the system just before the touching point (separated ions) and immediately after the touching point (compact system) is the same.

The time evolution of the collective degrees of freedom [deformation parameters $\mathbf{q} \equiv (\alpha,\alpha_1,\alpha_4)$] and the corresponding momenta $\mathbf{p}/\mathbf{m} \equiv (\dot\alpha,\dot\alpha_1,\dot\alpha_4)$ at both stages of the reaction are described by the stochastic Langevin equations [12], namely,

$$\begin{aligned}\dot q_\beta &= \mu_{\beta\nu}p_\nu,\\ \dot p_\beta &= -\frac{1}{2}p_\nu p_\eta\frac{\partial\mu_{\nu\eta}}{\partial q_\beta} + K_\beta - \gamma_{\beta\nu}\mu_{\nu\eta}p_\eta + \theta_{\beta\nu}\xi_\nu. \end{aligned} \quad (2)$$

Here $q_\beta$ are the deformation parameters, and a convention of summation over repeated indexes $\nu$, $\eta$ is used. The quantity $\gamma_{\beta\nu}$ is the tensor of friction coefficients and $\mu_{\beta\nu}$ is the tensor inverse to the mass tensor $m_{\beta\nu}$.

The random force $\theta_{\beta\nu}\xi_\nu$ takes into account the fluctuations in the system, where $\xi_\nu$ is a random number with the following properties:

$$\begin{aligned}\langle\xi_\nu\rangle &= 0,\\ \langle\xi_\beta(t_1)\xi_\nu(t_2)\rangle &= 2\delta_{\beta\nu}\delta(t_1 - t_2).\end{aligned} \quad (3)$$

The magnitude of the random force $\theta_{\beta\nu}$ is expressed in terms of the diffusion tensor $D_{\beta\nu}$, $D_{\beta\nu} = \theta_{\beta\eta}\theta_{\eta\nu}$, which is related to the friction tensor $\gamma_{\beta\nu}$ via the modified Einstein relation $D_{\beta\nu} = T^*\gamma_{\beta\nu}$. Here $T^*$ is the effective temperature introduced by H. Hofmann [13,14],

$$T^* = \frac{\hbar\varpi}{2}\coth\frac{\hbar\varpi}{2T}. \quad (4)$$

The point is that the classical Einstein relation $D = T\gamma$ is valid at relatively high temperatures. At low temperatures the quantal aspect of the fluctuation-dissipation becomes important and the magnitude of the diffusion coefficient becomes larger than its classical value; see [15,16].

This property is guaranteed by the form (4). Here parameter $\varpi$ is the local frequency of collective motion. In principle, it should be calculated at each deformation point. Unfortunately, this would be too time consuming. The value calculated in [17] of $\hbar\varpi$ at the ground state and the saddle of $^{224}$Th is close to 1 MeV. For the superheavies in the present calculations we used the somewhat larger value $\hbar\varpi = 2$ MeV independently of deformation ($T^* = 1$ MeV at $T = 0$).

The $T$ in (4) is the temperature related to the dissipated (excitation) energy by the Fermi-gas formula, $T = \sqrt{aE_{\rm dis}}$, with $a$ being the level density parameter [18]. The dissipated energy $E_{\rm dis}$ is calculated at each time step of Eqs. (2). It depends on the reaction energy $U^*$ and the kinetic and potential energy, namely,

$$E_{\rm dis} = U^* - \frac{1}{2}\sum_{\beta\nu}p_\beta p_\eta\mu_{\beta\eta} - V_{\rm pot}. \quad (5)$$

The reaction energy $U^*$ is related to the center-of-mass energy $E_{\rm cm}$ by the energy balance, $E_{\rm gs}(p) + E_{\rm gs}(t) + E_{\rm cm} = E_{\rm gs}(p + t) + U^*$, where $p$ and $t$ stand for the projectile and target nuclei. The $U^*$ can be expressed as $U^* = E_{\rm cm} - Q$, where $Q$ is so called $Q$ value of the reaction, $Q \equiv E_{\rm gs}(p + t) - E_{\rm gs}(p) - E_{\rm gs}(t)$. The $Q$ value is defined as the difference of ground state energies $E_{\rm gs}$; it does not depend on dynamics. For a particular reaction the ground state energies can be taken from existing tables or calculated, for example, within the macroscopic-microscopic approach.

The center-of-mass energy $E_{\rm cm}$ is fixed in the approaching phase. After formation of the compact system the energy available for the system is given by $E_{\rm cm} - Q$, i.e., by $U^*$. The reaction energy $U^*$ is shared between the collective kinetic energy and dissipated energy, which is released by the evaporation of particles and $\gamma$ quanta. For the second step of the fusion-fission reaction the use of $U^*$ is more convenient compared to $E_{\rm cm}$. In experimental works, at least in some of them (see [3]), the cross sections are given as functions of $U^*$.

The conservative force in (2) is represented by the derivative of free energy with respect to deformation, $K_\beta \equiv -\partial F/\partial q_\beta$, where $F(q,T) = V(q,T) - aT^2$. The potential energy of the compact system $V_{\rm pot}$ consists of the rotation and deformation $E_{\rm def}$ energies, i.e.,

$$V_{\rm pot} = \frac{\hbar^2L^2}{2J} + E_{\rm def}, \quad (6)$$

where $J$ is the rigid-body moment of inertia [19].

The nuclear deformation energy $E_{\rm def}$ is calculated within the macroscopic-microscopic method [20,21]. In this method the deformation energy is expressed as the sum of the macroscopic (liquid-drop) part $E_{\rm def}^{\rm LDM}$ and the shell correction $E_{\rm shell}$ (including the shell correction to the pairing correlation energy), i.e.,

$$E_{\rm def} = E_{\rm def}^{\rm LDM} + E_{\rm shell}. \quad (7)$$

For the macroscopic part we use the sum of surface and Coulomb energies with parameters given in [22]. The shell correction for protons ($p$) and neutrons ($n$) at zero excitation energy is calculated by the Strutinsky method [20,21]:

$$E_{\rm shell}(T = 0) = \sum_{p,n}(\delta E^{p,n} + \delta P^{p,n}). \quad (8)$$

The dependence of the shell correction on the temperature is given by the expression $E_{\rm shell}(T) = E_{\rm shell}(T=0)e^{-a\gamma T^2}$ [23]. The level density parameter $a$ and the shell correction damping parameter $\gamma$ are taken from [18].

Besides the deformation energy, the dynamic properties of each nucleus are characterized by the friction $\gamma_{\beta\nu}$ and inertia $m_{\beta\nu}$ tensors, which were calculated within the linear response approach and the local harmonic approximation [24,25]. In this approach, many quantum effects, such as shell and pairing effects, and the dependence of the collisional width of single-particle states on the excitation energy, are taken into account. The precise expressions for the friction $\gamma_{\beta\nu}$ and inertia $m_{\beta\nu}$ can be found in [26].

To start the second step calculations, we need information on the dependence of touching probability on the angular momentum of the system: the two-dimensional distributions of touching events in angular momentum and potential energy, and in angular momentum and excitation energy. All these data for the reactions considered here were calculated in [2]. The details of the transition from the first to the second step of the reaction can be found in [1,5].

On the second step of reaction the formation of the compound nucleus and evaporation residue can take place or the system can split back into two fragments. So, we calculate the evolution of the compact system either until it crosses the fission barrier and splits back into two fragments or until it gets deexcited by the emission of light particles and gamma rays and forms the evaporation residue.

In order to form the evaporation residue, the system should release the excitation energy by the evaporation of light particles and $\gamma$ quanta. The particle evaporation from an excited nucleus is described by statistical methods. We employ the method proposed in [18]; see also [27]. The probability for the emission of one particle or another depends on the decay width of the nucleus into particlar decay channel. The evaporation widths $\Gamma_j$ ($j \equiv n,p,d,t,^3{\rm He},\alpha$) and $\Gamma_\gamma$ are given by the expressions [18]

$$\Gamma_j = \frac{(2s_j+1)m_i}{(\pi\hbar)^2\rho_0(U_0)}\int_{Vj}^{U_j-B_j}\sigma_{\rm inv}(e)\rho_j(U_j-B_j-e)e\,de, \quad (9)$$

$$\Gamma_\gamma = \frac{1}{(\pi\hbar c)^2}\frac{1}{\rho_0(U_0)}\int_0^{U_0}\sigma_\gamma(e)\rho_j(U_0-E)e^2de. \quad (10)$$

Here, $\rho_0$, $\rho_j$, and $\rho_\gamma$ are the level densities, respectively, in the primary nucleus or in the nucleus formed after the particle or $\gamma$-quanta emission; $s_j$, $m_j$, $V_j$, $B_j$ are the spin of the emitted particle, its mass, the height of the Coulomb barrier, and its binding energy; $\sigma_{\rm inv}(e)$ is the cross section for the absorption of a particle or a $\gamma$ quanta with kinetic energy $e$ by the considered nucleus; $U_j = U - \Delta_j$; $U_0 = U - \Delta_0$; $U$ is the compound-nucleus excitation energy; and $\Delta_j$ and $\Delta_0$ are the pairing gaps for the residual and the primary nucleus, respectively.

After determining the widths for all evaporated particles, we find which particle, if any, is evaporated [28]. For this, we generate a random number $\xi$ between zero and unity and compare it with $\tau\sum\Gamma_b/\hbar$, where $\tau$ is the time step in numerically solving the Langevin equations (2). If this random number is smaller than $\tau\sum\Gamma_b/\hbar$, it is assumed that a particle is emitted at this step of solving the Langevin equations. The kind of a particle is determined again at random proportionally to the known width values.

If some particle is emitted, the binding energy of this particle is subtracted from the excitation energy of the system; the deformation energy and the transport coefficient are replaced by these for smaller particle number.

At low excitation energies the probability of particle ($\gamma$) evaporation becomes very low, consequently the calculation until the complete cooling of the system requires a lot of time. We stop the calculation for a given trajectory if the probability of the evaporation of any particle gets smaller than $10^{-3}$. In the reactions considered here mainly the neutrons are emitted. The number of emitted neutrons depends on the reaction energy $U^*$. The calculations show that at high values of $U^*$, $U^* =$ 50–60 MeV, up to five neutrons can be emitted.

At the beginning of the second step, the shape of the compact system consists of two ions connected by a thin neck. In the course of evolution, the neck can break down almost immediately after the touching (deep inelastic collision) or can get thicker; the system gets less elongated and moves (in the space of deformation parameters) toward the ground state. On this way the system has to overcome the fission barrier from outside (toward the ground state). If the system does not manage to overcome the fission barrier, it splits again into two fragments: quasifission takes place. If the system gets through the fission barrier, the fusion takes place. After the fusion the system can either get deexcited by the evaporation of $\gamma$ quanta or light particles and form the evaporation residue, or cross the fission barrier back (toward larger elongation). The last process is the true fission process. The outcome of the reaction depends on the random force $\theta_{\beta\nu}\xi_\nu$, which appears in the Langevin equations (2).

Repeating the calculation from the touching configuration many times, one gets probabilities of each particular process which is defined as the ratio of the number of trajectories leading to this process to the total number of trajectories. The relation between probabilities of different processes depends on the initial conditions (the shape of the initial system, especially, its mass asymmetry, angular momentum, and the kinetic, potential, and excitation energy at the touching point), on the value and deformation dependence of transport coefficients—potential energy and tensors of friction and inertia—and on the initial reaction energy $U^*$.

For comparison with the experimental data, the probabilities of fusion $P_{\rm comp}$ or evaporation residue formation $P_{\rm er}$ are transformed to corresponding cross sections:

$$\begin{aligned}\sigma_{\rm comp} &= \Sigma_L\sigma_{\rm comp}(L) = \Sigma_L P_{\rm comp}(L)\sigma_{\rm touch}(L),\\ \sigma_{\rm er} &= \Sigma_L\sigma_{\rm er}(L) = \Sigma_L P_{\rm er}(L)\sigma_{\rm touch}(L),\end{aligned} \quad (11)$$

where $\sigma_{\rm touch}(L)$ is the touching probability of the initial ions. These cross sections, calculated in [2] with and without inclusion of tunneling through the Coulomb barrier in the entrance channel, are shown in Fig. 1. The height of the Coulomb barrier depends on the reciprocal orientation of the projectile and target nuclei, their deformation, and the angular momentum. The arrows in Fig. 1 mark the value of $U^*$ which correspond to the highest Coulomb barrier at $L = 0$. At higher values of angular momentum the Coulomb barrier is even

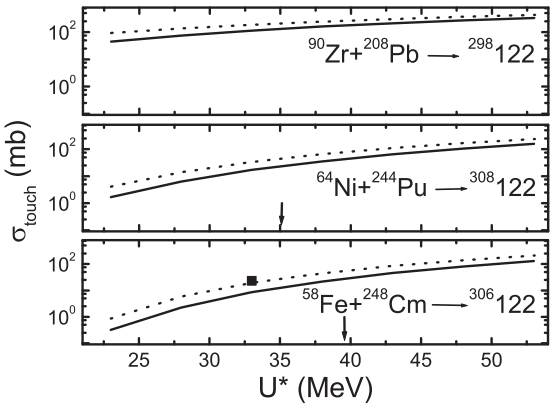


FIG. 1. The touching cross sections calculated in [2] for the reactions leading to the formation of system with charge number $Z = 122$. The calculations done with and without inclusion of tunneling through the Coulomb barrier are shown by dotted and solid lines respectively. The experimental value [3] is shown by ■. The arrows mark the value of $U^*$ which correspond to the highest Coulomb barrier at $L = 0$.

higher. At each value of $U^*$ some part of the trajectories can overcome the Coulomb barrier only due to the tunneling effect, and accounting for the tunneling effect increases the touching probability.

From the analysis of the approach phase of reactions leading to the synthesis of elements with $Z = 112, \ldots, 122$ in [2] it follows that the inclusion of the tunneling effect improves the agreement between the calculated and experimental values of the touching cross section. Consequently, the calculations below were carried out mainly using the initial data (touching point distributions) obtained with the inclusion of the tunneling effect in the entrance channel.

## III. THE EVOLUTION OF THE COMPACT SYSTEM

The main quantities of interest in the present calculations are the values of the fusion cross section and the evaporation residue cross section. To get these cross sections one has to calculate the time evolution of compact system. One of the main differences between the three considered reactions is the initial mass asymmetry of the compact system, which is characterized by the deformation parameter $\alpha_1$; see Fig. 2. In the reaction $^{58}\mathrm{Fe} + {}^{248}\mathrm{Cm} \to {}^{306-x}122 + xn$ the initial value of $\alpha_1$ is equal to 0.29, in the reaction $^{64}\mathrm{Ni} + {}^{244}\mathrm{Pu} \to {}^{308-x}122 + xn$ it is $\alpha_1^{(in)} = 0.23$, and $\alpha_1^{(in)} = 0.15$ in the reaction $^{90}\mathrm{Zr} + {}^{208}\mathrm{Pb} \to {}^{298-x}122 + xn$. It is seen from Fig. 2 that the initial point for the reaction $^{90}\mathrm{Zr} + {}^{208}\mathrm{Pb} \to {}^{298-x}122 + xn$ corresponds to the smallest potential energy.

In order for fusion to take place the shape of the compact system should evolve toward a smaller value of parameter $\alpha$ "climbing up" the slope of potential energy; see Fig. 2. This is possible due to the presence of a random force in Eqs. (2) and the available kinetic energy of radial motion.

The numerical value of the probability and corresponding cross section of reaching a certain value of $\alpha$ are calculated using equations similar to (11). The results of such calculations

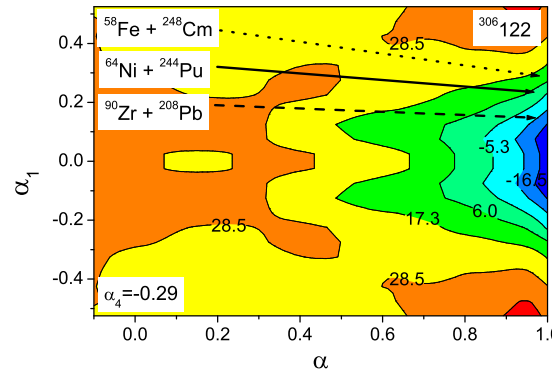


FIG. 2. The position of the starting point of the evolution of the compact system on the potential energy surface of isotope $^{306}122$, $V_{\mathrm{pot}}(\alpha_4 = -0.29, \alpha, \alpha_1)$ (in MeV).

are shown in Fig. 3. One can seen that on the way to fusion the fastest decrease of the survival probability takes place for the reaction with the smallest initial mass asymmetry, $^{90}\mathrm{Zr} + {}^{208}\mathrm{Pb} \to {}^{298-x}122 + xn$. Consequently, for this reaction the probability of reaching the ground state shape is the smallest.

The decrease of fusion cross sections slows down around $\alpha = 0.2$. One can believe that the trajectories which have reached the value $\alpha = 0.2$ contribute to the fusion process. Exactly in this region, $\alpha \approx 0.2$, is the position of the fission barrier; see Fig. 4. From the numerical results it follows that the fusion cross section for the reaction $^{90}\mathrm{Zr} + {}^{208}\mathrm{Pb} \to {}^{298-x}122 + xn$ is by 9–10 orders of magnitude smaller than that for reactions $^{58}\mathrm{Fe} + {}^{248}\mathrm{Cm} \to {}^{306-x}122 + xn$ and $^{64}\mathrm{Ni} + {}^{244}\mathrm{Pu} \to {}^{308-x}122 + xn$; see Fig. 3. Thus, further calculations for $^{90}\mathrm{Zr} + {}^{208}\mathrm{Pb} \to {}^{298-x}122 + xn$ make no sense.

From the comparison of the deformation dependence of fusion cross sections for different reaction energies $U^*$ in reaction $^{58}\mathrm{Fe} + {}^{248}\mathrm{Cm} \to {}^{306-x}122 + xn$, see Fig. 5, one can see that the fusion cross section decreases fast with decreasing $U^*$. On the other hand, for smaller values of reaction energy, the probability that the system would not undergo

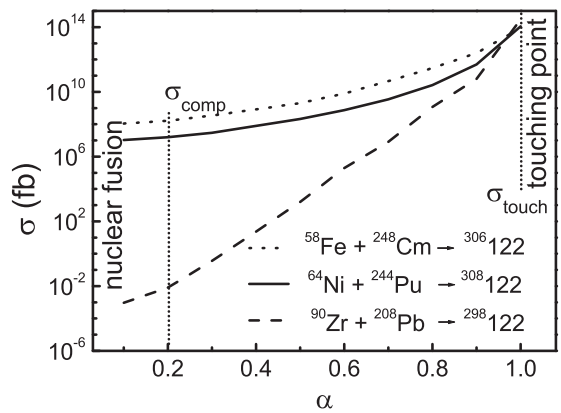


FIG. 3. The decrease of survival cross sections from the touching cross section ($\sigma_{\mathrm{touch}}$) at $\alpha = 1$ up to the fusion cross section ($\sigma_{\mathrm{comp}}$) at $\alpha \approx 0.2$ calculated for three different compact systems with the same reaction energy $U^* = 43$ MeV.

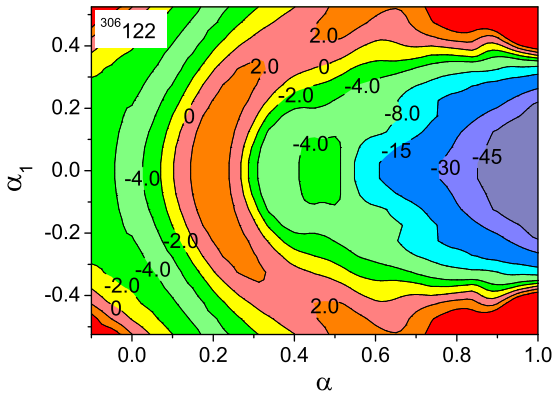


FIG. 4. The deformation energy [Eqs. (7) and (8)] of the compact system (in MeV) minimized with respect to $\alpha_4$.

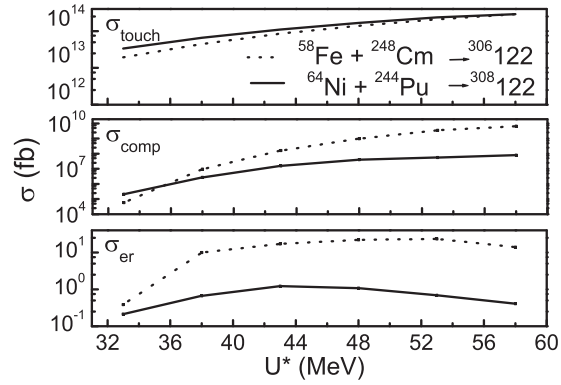


FIG. 6. The cross sections of touching ($\sigma_{\text{touch}}$), fusion ($\sigma_{\text{comp}}$), and evaporation residue formation ($\sigma_{\text{er}}$) in reactions $^{58}\text{Fe} + {}^{248}\text{Cm} \rightarrow {}^{306-x}122 + xn$ (dotted) and $^{64}\text{Ni} + {}^{244}\text{Pu} \rightarrow {}^{308-x}122 + xn$ (solid).

fission but would form the evaporation residue increases. Figure 6 shows the cross sections of touching, fusion, and evaporation residue formation in the reactions $^{64}\text{Ni} + {}^{244}\text{Pu} \rightarrow {}^{308-x}122 + xn$ and $^{58}\text{Fe} + {}^{248}\text{Cm} \rightarrow {}^{306-x}122 + xn$. It turns out that the touching cross section is larger in the reaction $^{64}\text{Ni} + {}^{244}\text{Pu} \rightarrow {}^{308-x}122 + xn$, but due to the different initial asymmetry of the compact system the fusion cross section is by 1.5 order of magnitude smaller than that for the reaction $^{58}\text{Fe} + {}^{248}\text{Cm} \rightarrow {}^{306-x}122 + xn$. The fission probability of isotopes $^{306-x}122$ is slightly larger than that of $^{308-x}122$. The evaporation residue formation cross sections for these two reactions differ only by one order of magnitude. At the reaction energy $U^* = 33$ MeV the cross sections are very close to each other.

Finally, we would like to examine the effect of tunneling through the Coulomb barrier in the entrance channel on the value of fusion cross section. To this end we compare in Fig. 7 the touching and fusion cross sections for the reaction $^{58}\text{Fe} + {}^{248}\text{Cm} \rightarrow {}^{306-x}122 + xn$ calculated with and without inclusion of tunneling. As one can see from the upper part of Fig. 7, the inclusion of tunneling increases the touching cross section by a factor of 5 or so at all values of the reaction energy $U^*$. The point is that the height of the Coulomb barrier in the entrance channel depends substantially on the deformation of the ions, their orientation in space, and their angular momentum. At each reaction energy $U^*$ some part of the trajectories can get through the Coulomb barrier only due to the tunneling effect. Thus, inclusion of the tunneling effect increases the touching cross section at all reaction energies.

The impact of the tunneling effect on the fusion probability at low and high reaction energy is quite different. The motion from the touching point toward the fusion region is mainly due to the available kinetic energy of radial motion. At low reaction energies both trajectories that overcame the Coulomb barrier with or without inclusion of tunneling effect have small velocity in the direction toward the ground state. The contribution of both type of trajectories to the fusion cross section is approximately the same. As one can see in the bottom part of Fig. 7, at low $U^*$ due to inclusion of tunneling the fusion cross section is increased by approximately a factor of 2. With growing $U^*$ the effect of tunneling gets smaller and smaller.

The trajectories which have reached the touching point due to the tunneling effect have kinetic energy in the direction toward the ground state that is close to zero. Such trajectories can overcome the fission barrier in the ground state direction

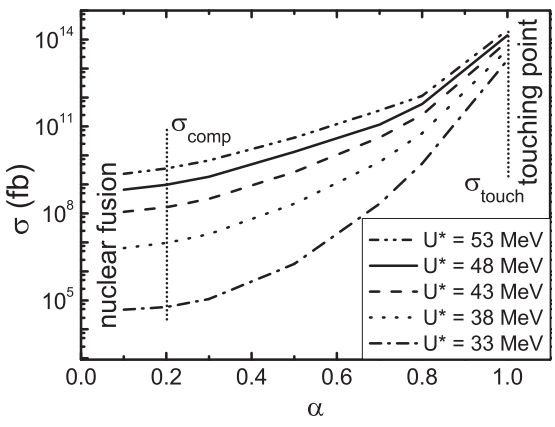


FIG. 5. The same as in Fig. 3 for different energies of the compact system formed in the reaction $^{58}\text{Fe} + {}^{248}\text{Cm} \rightarrow {}^{306-x}122 + xn$.

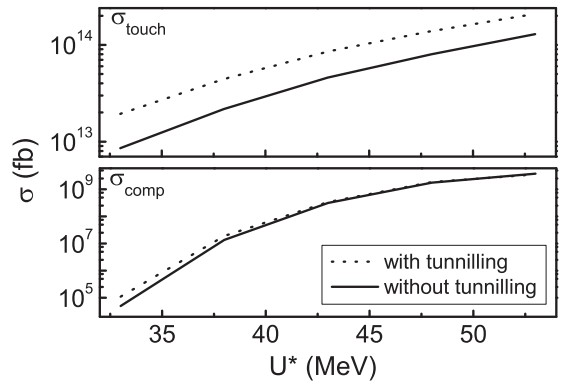


FIG. 7. The touching and fusion cross sections in the reaction $^{58}\text{Fe} + {}^{248}\text{Cm} \rightarrow {}^{306-x}122 + xn$, calculated with (dotted) and without (solid) inclusion of tunneling through the Coulomb barrier in the entrance channel.

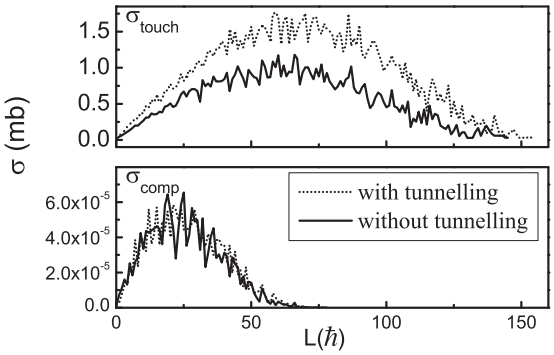


FIG. 8. The dependence of the touching and fusion cross sections on the angular momentum of the system in the reaction $^{58}\mathrm{Fe}+{}^{248}\mathrm{Cm}\rightarrow{}^{306-x}122+xn$ at the reaction energy $U^{*}=48$ MeV, calculated with (dotted) and without (solid) inclusion of tunneling through the Coulomb barrier in the entrance channel.

only due to the effect of the random force and eventually contribute to the deep inelastic scattering or quasifission.

At high reaction energies the part of trajectories which overcame the Coulomb barrier in the entrance channel without tunneling effect is larger. Some of these trajectories have large enough kinetic energy of radial motion in order to reach the ground state deformation. In other words, the contribution to fusion comes from trajectories which overcame the Coulomb barrier in the entrance channel without the tunneling effect. The contribution of the tunneling effect to the fusion cross section at height $U^{*}$ is negligibly small; see the bottom part of Fig. 7.

This conclusion is confirmed by the comparison of partial touching and fusion cross sections calculated with and without inclusion of the tunneling effect in the entrance channel at high reaction energy, shown in Fig. 8. The touching cross section calculated with inclusion of the tunneling effect is much larger than that calculated without inclusion of the tunneling effect, whereas the partial fusion cross sections in both cases are practically the same. Note that the trajectories with high angular momenta do contribute to the touching cross section but do not contribute to the fusion cross section.

In principle, in the description of the evolution of the compact system one has to account also for tunneling through the fission barrier. Unfortunately, tunneling in three-dimensional deformation space $\{\alpha,\alpha_1,\alpha_4\}$ is much more difficult to describe than tunneling through the one-dimensional Coulomb barrier. The investigation of tunneling through the fission barrier will be the subject of further studies.

## IV. SUMMARY

In present work we have calculated the fusion and the evaporation residue formation cross sections for the reactions $^{58}\mathrm{Fe}+{}^{248}\mathrm{Cm}\rightarrow{}^{306-x}122+xn$, $^{64}\mathrm{Ni}+{}^{244}\mathrm{Pu}\rightarrow{}^{308-x}122+xn$, and $^{90}\mathrm{Zr}+{}^{208}\mathrm{Pb}\rightarrow{}^{298-x}122+xn$ leading to the synthesis of isotopes of element $Z=122$. We have found out that the largest cross section is reached in the reaction with the most mass asymmetric combination of projectile and target nuclei, $^{58}\mathrm{Fe}+{}^{248}\mathrm{Cm}\rightarrow{}^{306-x}122+xn$. In this case the largest evaporation residue cross sections is equal to 23 fb at the initial reaction energy $U^{*}=53$ MeV ($E_{\mathrm{cm}}=299$ MeV).

It is shown that the trajectories which have reached the touching point due to tunneling effect through the Coulomb barrier in the entrance channel do not contribute to the fusion cross section.

[1] V. L. Litnevsky, V. V. Pashkevich, G. I. Kosenko, and F. A. Ivanyuk, Phys. Rev. C **85**, 034602 (2012).
[2] V. L. Litnevsky, G. I. Kosenko, and F. A. Ivanyuk, Phys. At. Nuclei **79**, 342 (2016).
[3] M. G. Itkis *et al.*, in *Proceedings of the International Symposium on Exotic Nuclei*, edited by Yu. E. Penionzhkevich and E. A. Cherepanov (World Scientific, Singapore, 2001), p. 143.
[4] V. L. Litnevsky, G. I. Kosenko, F. A. Ivanyuk, and V. V. Pashkevich, Phys. At. Nuclei **74**, 1001 (2011).
[5] V. L. Litnevsky, G. I. Kosenko, F. A. Ivanyuk, and V. V. Pashkevich, Phys. At. Nuclei **75**, 1500 (2012).
[6] V. L. Litnevsky, V. V. Pashkevich, G. I. Kosenko, and F. A. Ivanyuk, Phys. Rev. C **89**, 034626 (2014).
[7] T. I. Nevzorova and G. I. Kosenko, Phys. At. Nuclei **71**, 1373 (2008).
[8] C. W. Shen *et al.*, Sci. China Ser. G **52**, 1458 (2009).
[9] V. L. Litnevsky, G. I. Kosenko, F. A. Ivanyuk, and V. V. Pashkevich, Phys. At. Nuclei **75**, 37 (2012).
[10] V. V. Pashkevich, Nucl. Phys. A **169**, 275 (1971).
[11] V. V. Pashkevich, Nucl. Phys. A **477**, 1 (1988).
[12] Y. Abe, S. Ayik, P.-G. Reinhard, and E. Suraud, Phys. Rep. **275**, 49 (1996).
[13] H. Hofmann, C. Gregoire, R. Lucas, and C. Ngo, Z. Phys. A **293**, 229 (1979).
[14] H. Hofmann and D. Kiderlen, Int. J. Mod. Phys. E **07**, 243 (1998).
[15] H. Hofmann and F. A. Ivanyuk, Phys. Rev. Lett **82**, 4603 (1999).
[16] S. Ayik, B. Yilmaz, A. Gokalp, O. Yilmaz, and N. Takigawa, Phys. Rev. C **71**, 054611 (2005).
[17] H. Hofmann, F. A. Ivanyuk, C. Rummel, and S. Yamaji, Phys. Rev. C **64**, 054316 (2001).
[18] A. S. Iljinov, M. V. Mebel, N. Bianchi, E. De Sanctis, C. Guaraldo, V. Lucherini, V. Muccifora, E. Polli, A. R. Reolon, and P. Rossi, Nucl. Phys. A **543**, 517 (1992).
[19] R. W. Hasse and W. D. Myers, *Geometrical Relationships of Macroscopic Nuclear Physics* (Springer-Verlag, Heidelberg, 1988).
[20] V. M. Strutinsky, Nucl. Phys. A **95**, 420 (1967); **122**, 1 (1968).
[21] M. Brack, J. Damgaard, A. S. Jensen, H. C. Pauli, V. M. Strutinsky, and C. Y. Wong, Rev. Mod. Phys. **44**, 320 (1972).
[22] V. V. Pashkevich and A. Ya. Rusanov, Nucl. Phys. A **810**, 77 (2008).
[23] A. V. Ignatyuk, G. N. Smirenkin, and A. S. Tishin, Sov. J. Nucl. Phys. **21**, 255 (1975).

[24] H. Hofmann, Phys. Rep. **284**, 137 (1997).
[25] H. Hofmann, *The Physics of Warm Nuclei With Analogies to Mesoscopic Systems* (Oxford University Press, New York, 2008).
[26] F. A. Ivanyuk, in *Proceedings of International Conference on Nuclear Physics "Nuclear Shells-50"*, Dubna, Russia, 21–24 April 1999 (World Scientific, Singapore, 2000), p. 456.
[27] G. I. Kosenko, F. A. Ivanyuk, V. V. Pashkevich, and D. V. Dinner, Phys. At. Nuclei **71**, 2052 (2008).
[28] N. D. Mavlitov, P. Fröbrich, and I. I. Gontchar, Z. Phys. A **342**, 195 (1992).